LETTERS IN BIOMATHEMATICS
An International Journal

Intercollegiate Biomathematics Alliance

RESEARCH ARTICLE

OPEN ACCESS

A Discrete Age Structured Model of Hantavirus in a Rodent Reservoir in Paraguay

Morganne Igoe[a], E. Joe Moran[b], Theresa R. Sheets[c], Jeff DeSalu[d], Colleen B. Jonsson[e], Suzanne Lenhart[a,f], Robert D. Owen[g,h], Megan A. Rúa[i]

[a]Department of Mathematics, University of Tennessee, Knoxville, TN; [b]Department of Ecology, Pennsylvania State University, University Park, PA; [c]Department of Mathematics, University of Utah, Salt Lake City, UT; [d]Ecology and Evolutionary Biology Department, University of Tennessee, Knoxville, TN; [e]Department of Microbiology, Immunology, and Biochemistry, U. of Tennessee Health Sciences Center, Memphis, TN; [f]National Institute for Mathematical and Biological Synthesis, Knoxville, TN; [g]Department of Biological Sciences, Texas Tech University, Lubbock, TX; [h]Centro para el Desarrollo de Investigación Científica, Asunción, Paraguay; [i]Department of Biological Sciences, Wright State University, Dayton, OH

ABSTRACT

Many rodent-borne hantaviruses are zoonotic pathogens that can cause disease in humans through inhalation of aerosolized rodent excreta. To evaluate the prevalence of Jaborá virus (JABV) over time within its rodent reservoir, *Akodon montensis*, we formulated a mathematical model with multiple rodent age classes and unique infection class progression features. We then parameterized the model with data collected from a survey of JABV harbored by *Akodon montensis* in the Mbaracayú Reserve in Paraguay. Our model incorporates three types of infection over the lifetime of the rodent as well as a recovered class. A new feature of the model allows transition from the latent to the persistently-infected class. With a more complete age and infection structure, we are better able to identify the driving forces of epidemiology of hantaviruses in rodent populations.

ARTICLE HISTORY
Received June 14, 2020
Accepted August 21, 2020

KEYWORDS
epidemiological model, hantavirus in rodents, discrete time, age structure

1 Introduction

Hantaviruses are endemic in most parts of the world, being harbored by rodents, bats, moles or shrews. Each mammalian reservoir carries a unique viral strain. Intraspecies transmission occurs through the inhalation of aerosolized virus excreted in urine or feces (Padula et al., 2004), or through an exchange of blood and saliva during aggressive encounters among conspecific individuals (Glass et al., 1988). We note that hantavirus is not lethal in rodents and does not usually cause health issues. While not widely studied for most hantaviral reservoirs, viral infection of some rodent reservoirs may show lower survival rates, lower body mass, slower weight gains, and higher testosterone (for example, see Luis et al. (2010, 2012)). However, no pathology has been observed in bank voles infected with Puumala virus (Yanagihara et al., 1985), in deer mice experimentally infected with Sin Nombre virus (Botten and Fix, 2000), or in cotton rats infected with Black Creek Canal virus (Hutchinson et al., 2000). But higher doses of Black Creek Canal virus in the cotton rat can cause pneumonitis (Hutchinson and Fix, 1998). Researchers have reported that Sin Nombre virus (SNV) seroprevalence may vary from very low (<1%) to levels greater than 25% in long-term sampling in the western United States (Calisher et al., 2007). Field studies in Chile by Padula et al. (2004) suggested that a latency period may be responsible for the low prevalence.

Rodent reservoirs of Jaborá hantavirus in *Akodon montensis* have been studied in the Interior Atlantic Forest of Paraguay, and these populations exhibited low prevalence levels (Eastwood et al., 2018; Owen et al., 2010). To mechanically explain the low prevalence of JABV over time within its rodent reservoir, *A. montensis*, we propose a mathematical model with rodent age classes and a unique 'latency' class (having the virus but without the ability to transmit it). While the model used in this paper is based on data from JABV found in a South American rodent reservoir, *A. montensis* in Paraguay, the model is generalizable to other rodent reservoirs of hantaviruses due to its structure with age and infection classes (Jonsson et al., 2010; Yates et al., 2002).

Upon infection, the rodent reservoir can be characterized as having an acute infection as demonstrated by virus being shed

CONTACT Morganne Igoe migoe@utk.edu

in urine and feces. At some point, the rodent transitions to a persistent infection which is characterized by low or undetectable levels of virus being shed in urine or feces. However the rodent remains infected in many tissues such as the lung and heart (for example, see Botten and Fix (2000); Green and Fix (1998)). Such persistently infected rodents do not clear the virus, as documented in McAllister and Jonsson (2014), and this feature will be represented in our model. It is through these cycles that rodent-borne hantaviruses are maintained in rodent communities in nature.

Infection of humans by exposure to rodent-borne viruses is considered to be a dead end, since humans cannot transmit the virus to one another (LeDuc et al., 2002). In the New World, some hantavirus species transmitted from rodents to humans cause hantavirus pulmonary syndrome, a serious condition with basic life support as the only medical treatment and mortality rates of 36% in the United States (CDC, 2016). To better understand the drivers behind hantavirus spread, both intraspecies and interspecies transmission must be considered. Prevalence levels for hantavirus infection within rodent host populations vary seasonally and geographically, ranging from roughly 1 to 6% in the montane grass mouse, *A. montensis*, in Brazil and Paraguay, to 1 to 30% documented in the deer mouse, *Peromyscus maniculatus*, in the United States (Teixeira et al., 2014; Childs et al., 1994). A suite of factors drives viral prevalence in rodent populations including host genetics, mating behaviors and environmental factors (Luis et al., 2010; Eastwood et al., 2018). For example, the species *A. montensis* does not enter torpor (a short period of reduced body temperature and metabolic activity), and can have up to three reproductive cycles each year, potentially leading to higher population density and/or higher dispersal rates (Jordão et al., 2010; Owen et al., 2010). Both factors would likely increase contact and agonistic encounters with both conspecifics and other species. This contrasts with North American rodent species such as *P. maniculatus* which undergo torpor and have only a single reproductive cycle each year. Together these and other abiotic and biotic factors modulate viral prevalence observed in males and females. Environmental characteristics, such as seasonality and landscape structure, have also been linked to increased prevalence, as have anthropogenic factors such as ecological disturbance and its corresponding impact on biodiversity (Luis et al., 2010; Langlois et al., 2001; Lehmer et al., 2008).

Previous theoretical work in this system has incorporated differences in transmission and environmental factors to understand changes in overall virus prevalence. Allen and collaborators have published several papers on epidemiological models of hantavirus in *A. montensis* in Paraguay (Allen, McCormack, and Jonsson, 2006; Allen et al., 2009; Wesley et al., 2009). These models include

- a 2006 differential equations model followed by a stochastic model with SEIR compartments (susceptible, exposed, infected, recovered) to include random seasonal and environmental variations (both in Allen, Allen, and Jonsson (2006));
- a 2006 differential equations model featuring separate sex classes, followed by a stochastic differential equations model of similar structure (both in Allen, McCormack, and Jonsson (2006));
- a 2009 model by Allen et al. (2009) which used a habitat-based model for the spread of hantavirus between a reservoir and spillover species; and
- a 2010 model by Wesley et al. (2010) that used an SI model which includes two infected classes and examines the role of viral-contaminated soil.

Despite the extensive modeling work previously completed in this system, there has only been one discrete model developed to investigate the outbreak structure for viral transmission of hantavirus (Wesley et al., 2009). This model consists of a discrete-time rodent-hantavirus model structured by two infected classes (one for males and one for females) and three age classes. It includes juveniles, subadults, and adults, split into female and male groups, and susceptible and infected classes of adults. It further assumes that the juveniles and subadults could not become infected, and focuses on differences in contact rates based on the sex of the mice. Due to age structure in our data set, we chose to formulate a model discrete in time with three age classes and to use three types of infected classes to investigate persistent low levels of prevalence. We include a 'latent' class, which cannot transmit the virus but carries it, which was suggested by the work of Padula et al. (2004). Our model also differs from other hantavirus models due to its strong connection to data from Paraguay (Eastwood et al., 2018).

Motivated by the extensive prevalence data for hantaviruses in rodents collected in August 2014 in the Mbaracayú Reserve in Paraguay (Eastwood et al., 2018), and by the fluctuations in prevalence but persistence of the virus at a low level in data collected from the region in 2005–2006 (Owen et al., 2010), we investigated possible mechanisms for the observed occurrences of the virus through modeling. Our model is an age structured, discrete model which incorporates latent and recovered classes, and our transition rates and prevalence levels are directly connected to this data (Eastwood et al., 2018) in Paraguay. In addition to the classical stages of infection, acute and persistent, we add a latent class to better examine the dynamics of the virus. In this model, rodents in the latent class do not shed virus, so they are not transmitting the virus, but are able to transition back into the persistently infected class. The latent class is a novel addition to our model (compared to previous models), which offers a possible explanation for the maintenance of the virus during normal periods and periods when outbreaks of virus are driven by biotic or abiotic factors. The age structure includes differing transmission coefficients between juvenile and adult populations. By incorporating the new latent class and an expanded age class structure into our model, we address the dynamics of hantavirus within rodent populations.

In the next section, we describe our data and our model. Then we follow with results and discussion, and in the last section, conclusions are given.

2 Methods

2.1 Our Data

Our model is based on data collected in August 2014 in the Reserva Natural de Bosque Mbaracayú (RNBM) in Paraguay (Eastwood et al., 2018). The data collected at 22 sites from 2–11 nights of trapping include 417 rodents. Recorded features included species, weight, total length, sex, reproductive status and categorical age. For all species, a combination of pelage (fur), size, behavior and *gestalt* was used to designate age class. The presence of rodent-borne hantavirus antibodies and/or RNA and characteristic tail lesions (potentially due to Leishmania) were also collected. Because we were interested in rodents which serve as the main vector for hantavirus, we extracted species data for the most prevalent hantaviral reservoir species, *A. montensis* (sample size=274), which comprised about 70% of the collected rodents. Three of the 274 *A. montensis* were newborns so sex on these animals could not be determined and were therefore excluded from further analysis. Overall, we had 271 rodents in our dataset.

The demographic makeup of our data set (Eastwood et al., 2018) was 52% male, 48% female, 83% adults, and 17% juvenile. The overall hantavirus prevalence was 6%, which is close to that in other studies (Eastwood et al., 2018; Owen et al., 2010; Muylaert et al., 2019). Of the entire population, 7% of the males had hantavirus, and 3% of the females had hantavirus. Within recorded hantavirus cases, 71% occurred in males, while 29% occurred in females. For the entire population, the prevalence among juveniles was 6% and the prevalence among adults was 5%. Among seropositive individuals, juveniles compose 21%, and adults compose 79%.

2.2 Our Model

In our model, the population is divided into three age classes (listed with lengths of time in each class): newborns B (23 days), juveniles J (37 days), and subadults and adults A (305 days). There was not enough data to adequately separate subadults and adults so they were combined into one class. These classes include males and females, homogeneously mixed. The susceptible population S is broken into two compartments: susceptible juveniles S_J and susceptible adults S_A. The literature suggests that newborns may be unable to become infected or may be delayed in their rate of infection due to maternal antibodies (Voutilainen et al., 2016; Kallio et al., 2013, 2010; Dearing et al., 2009; Georges et al., 2008; Kallio et al., 2006; Borucki et al., 2000; Bernshtein et al., 1999; Dohmae and Nishimune, 1998) and/or their decreased contact with infected individuals due to their limited movement from the den and mother, but the study by Hutchinson et al. (2000) did not observe the influence of maternal antibodies on infection in Black Creek Canal virus. In our model, the newborns B are not susceptible and cannot be infected until they become juveniles. The acutely infected population is broken into two compartments: infected juveniles I_J and infected adults I_A which have been reported to have the highest probability of shedding virus in saliva and excreta. As with the majority of viral infections, rodents within this class will not produce antibodies early during the course of infection, and begin in some reservoirs approximately ten days post-infection (Schountz et al., 2012, 2014). Once antibodies are produced in response to the infection, fewer free virions will be available to infect other rodents.

The persistently-infected population is broken into two compartments: persistently-infected juveniles P_J and persistently infected adults P_A. Persistently-infected rodents shed fewer virions and are significantly less infectious than I_A and I_J populations and therefore have a lower transmission rate, and note that only the I_A class can move to recovered R. The latent class L and recovered class R consist only of adults. Rodents in the latent class L do not shed virus but are able to regress back into the persistently infected stage P_A. The recovered class R is not able to transmit the pathogen and is unable to regress back into an infected class. Figure 1 illustrates the possible infection status and age transitions of the model shown in equations (1)–(9). The periods of time in each infected class and age class are shown in Table 1 and Figure 2.

The model is stated in equations (1)–(9), where the adult population is $A(t) = S_A(t) + I_A(t) + P_A(t) + L(t) + R(t)$. The model is discrete in time, using time-steps of days. The order of events in this model is: survival, age transition out of class, age transition into class, new infection, progression of infection out of class, and progression of infection into class. Transition from P to L_A happens last. The parameters of the model are defined in Table 2. All age transition rates are denoted by μ_B, μ_J, and μ_A for the three classes (newborns, juveniles and adults).

We discuss each equation in the model in detail. Given a death rate, like d_B, then the corresponding survival rate is $(1-d_B)$, and given a transition rate out of a compartment, like μ_B, the corresponding rate for remaining in that compartment is $(1-\mu_B)$. Starting with the newborn class $B(t)$, the survival and the remaining in class have coefficients $(1-d_B)$ and $(1-\mu_B)$. Then lastly, the new births are added in with density dependence on the size of the adult population $A(t)$, which is shown with a baseline

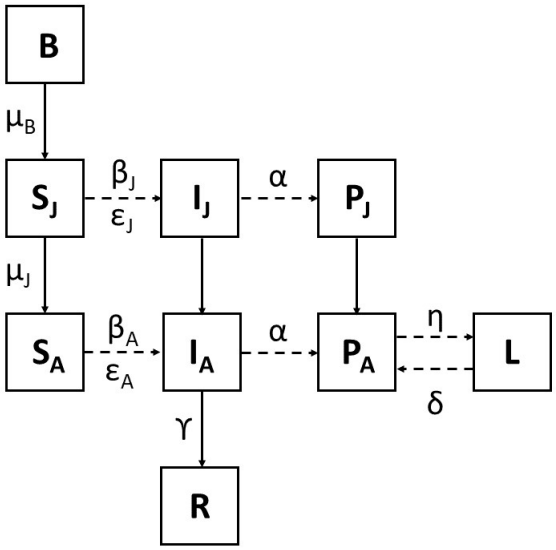

Figure 1: A flowchart of the model shown in equations (1)–(9). Vertical arrows denote age transitions and horizontal arrows denote infection transitions. Births from the adults, $S_A + I_A + P_A + L + R$, come into the newborn class B. Natural deaths occur from each compartment, but note that there are no pathogen induced deaths.

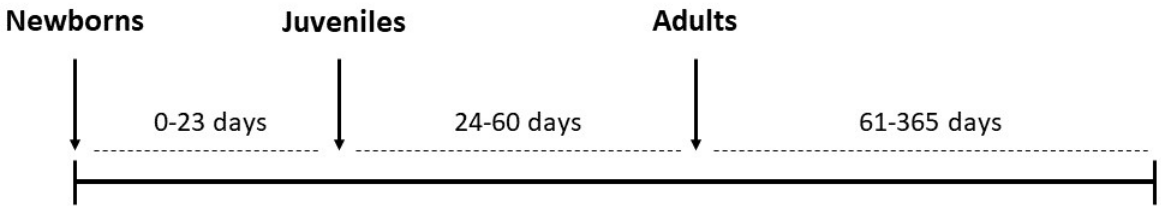

Figure 2: Timeline progression from newborn to adult. Time is measured in days post birth.

Table 1: Table of infection classes, transmission levels, and infection class length in days.

Class	Level of Infectiousness	Length (days)
Acutely Infected (I)	Shedding most virus	23
Persistently Infected (P)	Shedding little virus	37
Latent (L)	No Shedding	60

rate b_A and modified by

$$\frac{K}{K + A(t)}.$$

Note the birth rate b_A will be one half of the birth rate for females in our population, assuming that there are equal numbers approximately of males and females. The order of events in the S_J equation begins with the individuals of $S_J(t)$ surviving with rate $(1 - d_J)$ and remaining after age transition with rate $(1 - \mu_J)$. This is followed by adding individuals due to age transition from newborn to juvenile, represented by $(1 - d_B)\mu_B B(t)$. These actions in the S_J equation are followed by transmission, which moves a proportion of individuals from S_J to I_J, with corresponding β and ε terms in the exponential term, due to transmission from I_J, I_A, P_J, and P_A classes. The proportion of the S_J class remaining is

$$\exp\Big(-\big(\beta_{JJ} I_J(t) + \beta_{AJ} I_A(t) + \varepsilon_{JJ} P_J(t) + \varepsilon_{AJ} P_A(t)\big)\Big)$$

after the following proportion moves to I_J due to transmission

$$1 - \exp\Big(-\big(\beta_{JJ} I_J(t) + \beta_{AJ} I_A(t) + \varepsilon_{JJ} P_J(t) + \varepsilon_{AJ} P_A(t)\big)\Big).$$

Then looking to the I_J class, we see the three factors $(1 - d_J)(1 - \mu_J)(1 - \alpha)$ representing the proportion of $I_J(t)$ surviving with $(1 - d_J)$, remaining after age transition with $(1 - \mu_J)$ and remaining after transition to P with $(1 - \alpha)$. Then, infecteds from S_J move into this class with the $(1 - \exp(\ldots))$ term. The last juvenile class P_J has the rates of surviving and remaining after age transition as $(1 - d_J)(1 - \mu_J)$. A proportion of the I_J individuals, who have survived and remain juvenile, make their transition into P_J with rate α, given by $I_J(t)(1 - d_J)(1 - \mu_J)\alpha$.

Similarly for the adult classes, we have S_A individuals surviving with rate $(1 - d_A)$ and then individuals of the S_J class moving in due to age transition as $(1 - d_J)\mu_J S_J$. The proportion remaining after transmission is represented by the $\exp(-\ldots)$ with corresponding coefficients $\beta_{JA}, \beta_{AA}, \varepsilon_{JA}$, and ε_{AA}. The I_A equation is similar to the I_J equation, except for transition in from the I_J compartment and followed by transition γ out to the R class.

The P_J equation has survival $(1 - d_J)$ and the proportion $(1 - \mu_J)$ remaining after the transition to P_A, followed by the transition from I_J with the term

$$I_J(t)(1 - d_J)(1 - \mu_J)\alpha.$$

The P_A equation has survival and the addition of the transitioning P_J individuals, followed by the transition to the L class, and then the transition from I_A (with rate α) and from L (with rate δ).

The L class has survival, transition in from P_A (with rate η) and then the remaining proportion $(1 - \delta)$ after a proportion δ moves to P_A. Lastly the recovered class R survives, and then there is movement in from I_A with terms

$$\gamma(1 - \alpha)\Big(I_A(t)(1 - d_A) + I_J(t)(1 - d_J)\mu_J\Big),$$

as can be seen in the last term in the following system of equations:

$$B(t+1) = B(t)(1 - d_B)(1 - \mu_B) + \frac{b_A K}{K + A(t)} A(t) \tag{1}$$

$$S_J(t+1) = \Big(S_J(t)(1 - d_J)(1 - \mu_J) + B(t)(1 - d_B)\mu_B\Big) \exp\Big(-\big(\beta_{JJ} I_J(t) + \beta_{AJ} I_A(t) + \varepsilon_{JJ} P_J(t) + \varepsilon_{AJ} P_A(t)\big)\Big) \tag{2}$$

$$S_A(t+1) = \Big(S_A(t)(1 - d_A) + (1 - d_J)\mu_J S_J(t)\Big) \exp\Big(-\big(\beta_{JA} I_J(t) + \beta_{AA} I_A(t) + \varepsilon_{JA} P_J(t) + \varepsilon_{AA} P_A(t)\big)\Big) \tag{3}$$

$$\begin{aligned} I_J(t+1) = {} & I_J(t)(1 - d_J)(1 - \mu_J)(1 - \alpha) \\ & + \Big(S_J(t)(1 - d_J)(1 - \mu_J) + B(t)(1 - d_B)\mu_B\Big)\Big(1 - \exp\Big(-\big(\beta_{JJ} I_J(t) + \beta_{AJ} I_A(t) + \varepsilon_{JJ} P_J(t) + \varepsilon_{AJ} P_A(t)\big)\Big)\Big) \end{aligned} \tag{4}$$

$$\begin{aligned} I_A(t+1) = {} & \Big(I_A(t)(1 - d_A) + I_J(t)(1 - d_J)\mu_J\Big)(1 - \alpha)(1 - \gamma) \\ & + \Big(S_A(t)(1 - d_A) + S_J(t)(1 - d_J)\mu_J\Big)\Big(1 - \exp\Big(-\big(\beta_{JA} I_J(t) + \beta_{AA} I_A(t) + \varepsilon_{JA} P_J(t) + \varepsilon_{AA} P_A(t)\big)\Big)\Big) \end{aligned} \tag{5}$$

$$P_J(t+1) = P_J(t)(1 - d_J)(1 - \mu_J) + I_J(t)(1 - d_J)(1 - \mu_J)\alpha \tag{6}$$

$$\begin{aligned} P_A(t+1) = {} & \Big(P_A(t)(1 - d_A) + (1 - d_J)\mu_J P_J(t)\Big)(1 - \eta) \\ & + \Big(I_A(t)(1 - d_A) + I_J(t)(1 - d_J)\mu_J\Big)\alpha + \delta\Big(L(t)(1 - d_A) + \eta\Big(P_A(t)(1 - d_A) + P_J(t)(1 - d_J)\mu_J\Big)\Big) \end{aligned} \tag{7}$$

$$L(t+1) = \Big(L(t)(1-d_A) + \eta\Big(P_A(t)(1-d_A) + P_J(t)(1-d_J)\mu_J\Big)\Big)(1-\delta) \tag{8}$$

$$R(t+1) = R(t)(1-d_A) + \gamma(1-\alpha)\Big(I_A(t)(1-d_A) + I_J(t)(1-d_J)\mu_J\Big) \tag{9}$$

3 Results and Discussion

The parameters of the model are defined in Table 2.

All age transition and infected class progression rates are in terms of days and are the reciprocal of the length of time an individual spends in each age or infected class (Figure 2, Table 1). Mortality rates were estimated using those rates for a single season in Galiano et al. (2011); Gentile et al. (2000). Mortality rates were then derived using the length of time of each age class and overall mortality rate for a season, with mortality in the newborn phase being low, juvenile high, and adult moderate (Gentile et al., 2000). Assuming half the adults are female, the baseline birth rate b_A would be one half of the birth rate from females. Note that $b_A = \frac{1}{70} = 0.0143$ births per day would result in about 10.5 newborns in year, usually coming from 2 or 3 litters per female per year (Eastwood et al., 2018; Owen et al., 2010).

The parameters for the infected classes were derived from seroprevalence data showing days past infection (Lee et al., 1982). The rates are the reciprocals of these infectious periods. Age class progression rates were derived from (Gentile et al., 2000) by taking the reciprocal of the time within an age class. The parameter β_{AA} was manipulated to achieve an equilibrium prevalence of 6% to match our data set and what was observed in other *A. montensis* populations (Teixeira et al., 2014). The other transmission rates are expressed as fractions of the baseline transmission rate β_{AA}.

To determine the baseline population from which simulations for the model were run, we first calculated the disease free equilibrium (DFE) (from equations (10)–(12)) by assuming that $I_J = I_A = P_J = P_A = L = R = 0$, and deriving expressions for the non-infected classes (B, S_J, and S_A) shown in equations (10)–(12). We then expressed the initial conditions for the infected classes as a proportion of the total population at the disease free equilibrium. The multipliers were chosen to achieve approximately a 6% overall prevalence in the initial population, as was observed in the data collected in the Mbaracayú Reserve. For example, we calculated from the data that approximately 60% of individuals in the infected classes belonged to the infected class I, while approximately 30% of the individuals were in the persistently infected class P. Additionally, we estimated that approximately 21% of the individuals in the infected classes were juveniles, while about 79% were adults. Lastly, we estimated that 10% of the infected population belonged to the latent class L based on the data set (Eastwood et al., 2018) and a prior study (Owen et al., 2010). These approximations were used to create the initial conditions for the infected classes shown in equations (16)–(21). Any alterations to the model parameters in a simulation were recorded and the initial conditions were recalculated under these new conditions. This was done in order to standardize initial conditions for the parameter changes.

$$B^* = \frac{K[b_A(1-d_J)\mu_J(1-d_B)\mu_B - d_A(1-(1-d_B)(1-\mu_B))(1-(1-d_J)(1-\mu_J))]}{(1-(1-d_B)(1-\mu_B))(1-d_J)\mu_J(1-d_B)\mu_B} \tag{10}$$

$$S_J^* = \frac{B^*(1-d_B)\mu_B}{(1-(1-d_J)(1-\mu_J))} \tag{11}$$

$$S_A^* = \frac{(1-d_J)\mu_J S_J^*}{d_A} \tag{12}$$

$$B(0) = B^* \tag{13}$$

$$S_J(0) = S_J^* \tag{14}$$

$$S_A(0) = S_A^* \tag{15}$$

$$I_J(0) = (0.06 * 0.6 * 0.21)(B^* + S_J^* + S_A^*) \tag{16}$$

$$I_A(0) = (0.06 * 0.6 * 0.79)(B^* + S_J^* + S_A^*) \tag{17}$$

$$P_J(0) = (0.06 * 0.3 * 0.21)(B^* + S_J^* + S_A^*) \tag{18}$$

$$P_A(0) = (0.06 * 0.3 * 0.79)(B^* + S_J^* + S_A^*) \tag{19}$$

$$L(0) = (0.06 * 0.1)(B^* + S_J^* + S_A^*) \tag{20}$$

$$R(0) = 0 \tag{21}$$

The Next Generation Matrix Method for calculating the basic reproduction number R_0 for discrete-time models described by Allen and van den Driessche (2008) was used to calculate R_0 for the model; we checked the needed assumptions to use this method on our model (meaning, the spectral radius of the Jacobian of the transitions between infected classes and of the Jacobian for the model without infection are both below 1.) Using this method, we take the infected classes to I_J, I_A, P_J, P_A, L and then R_0 takes the form $R_0 = \rho(F(I-T)^{-1})$, where F is the Jacobian matrix that results from differentiating the terms that describe new infections in the infected classes, T is the Jacobian matrix that results from differentiating all other transitions in the infected classes, and ρ is the spectral radius. This method allowed for the simplification of the system to five equations by limiting calculations to only equations (4)–(8); those pertaining to infected individuals. We used the block structure, determinants, traces, and sum of minors, but we were not able to find a reasonable algebraic expression for R_0. Thus R_0 was only calculated for our particular parameter values, shown in Table 2, yielding $R_0 = 1.06$. This indicates that the DFE is unstable and the infection persists in our model.

We ran model simulations with the baseline parameters, which gave the initial conditions stated in equations (22)–(30). The total initial population is 652, of which 37 are infected and 616 non-infected. Figure 3 shows all the noninfecteds in the population. The susceptible adult S_A compartment decreases from 479 to 418, while the newborn B compartment increases. The susceptible juvenile S_J and recovered R compartments appear to be leveling off. In Figure 4, we see the five infected compartments with P_J, P_A, and L increasing at first and with I_J and I_A both decreasing. The prevalence starts at about 5.6% and drops only slightly over time to 4.9% over a year.

$$B(0) = 64.3684 \tag{22}$$
$$S_J(0) = 71.8341 \tag{23}$$
$$S_A(0) = 479.4815 \tag{24}$$

$$I_J(0) = 4.6546 \tag{25}$$
$$I_A(0) = 17.5101 \tag{26}$$
$$P_J(0) = 2.2165 \tag{27}$$
$$P_A(0) = 8.7550 \tag{28}$$

$$L(0) = 3.6941 \tag{29}$$
$$R(0) = 0 \tag{30}$$

In order to assess the relationship between prevalence and the model parameters, we performed a Latin Hypercube Sensitivity Analysis (Marino et al., 2009). This analysis randomly generates a matrix of 10,000 vectors of the model parameters within given bounds, which were chosen as 25% above and below the baseline parameters. Using parameters $\beta_{AA}, b_A, d_B, d_J, d_A, u_J, \alpha, \gamma, \eta$, and δ, we verified that the monotonicity of the output measure of prevalence with respect to each parameter, which is needed to use the Partial Rank Correlation Coefficients (PRCC). Simulations were then run using each vector of the parameters, with the output measure of prevalence after 300 time-steps. A PRCC and a p-value are then produced for each model parameter. The sign and magnitude of the correlation coefficient, as well as the p-value, were used to assess the impact and statistical significance of each parameter on the prevalence of the virus within the population. Using this analysis, we found that all parameters were statistically significant, having p-values below 0.05 (Figure 5). Note that the baseline birth and death rates, b_A and d_A, are known from this data and we do not need to further investigate its effect. If the rodents recover, then they do not get into the loop for P_A and L, and thus we will choose to vary the recovery rate γ to document its effect on prevalence. We will vary the transition rates, δ and η, between classes L and P_A.

To test how prevalence is affected by changes in the initial rodent population, the model was simulated at the baseline values. The model was simulated four times, each time varying the initial condition of one of the compartments B, L, I_A, S_j, at ten times its baseline initial condition value while keeping all other initial values at the baseline (Figure 6). For example, if the baseline value for infected adults was 1, a simulation would be run in which the initial number of infected adults was 10 and all other initial values were maintained at the baseline. This gives a comparison of how differences in the initial population of a particular class affect the prevalence of the virus. When varying the age structure of the population in our model, prevalence was found to be more sensitive to increases in the initial number of individuals in the younger age classes (Figure 6). When newborns and susceptible juveniles are the age class with the largest initial population, the prevalence of hantavirus spikes and eventually returns to the baseline. When the dominant initial age class is comprised of adults, the spike in prevalence is much lower and the prevalence returns to the baseline in a shorter amount of time than when the younger age classes are initially dominant. This is of particular importance during conditions that are conducive to newborn and juvenile success such as high resource availability or lack of predators.

Table 2: Table of parameter definitions and values. All the rates have units of per day, the time-step. The parameter K has units of number of rodents.

Parameter	Definition	Value
μ_i	Transition rate from age class i	$\mu_B = 1/23$ $\mu_J = 1/37$
d_i	Death rate for age class i	$d_B = 0.003521$ $d_J = 0.012123$ $d_A = 0.004$
α	Rate of transition from I to P class	$1/23$
γ	Rate of recovery	$1/10$
η	Rate of transition from P to L class	$1/37$
δ	Rate of transition from L to P class	$1/60$
β_{ij}	Transmission rate for I class	$\beta_{AA} = \beta_{JJ} = 0.00012$ $\beta_{AJ} = \beta_{JA} = 0.75 * \beta_{AA}$
ε_{ij}	Transmission rate for P class	$\varepsilon_{AA} = \varepsilon_{JJ} = 0.25 * \beta_{AA}$ $\varepsilon_{AJ} = \varepsilon_{JA} = 0.1875 * \beta_{AA}$
K	Density dependent effect on births	375
b_A	Birth rate	0.0143

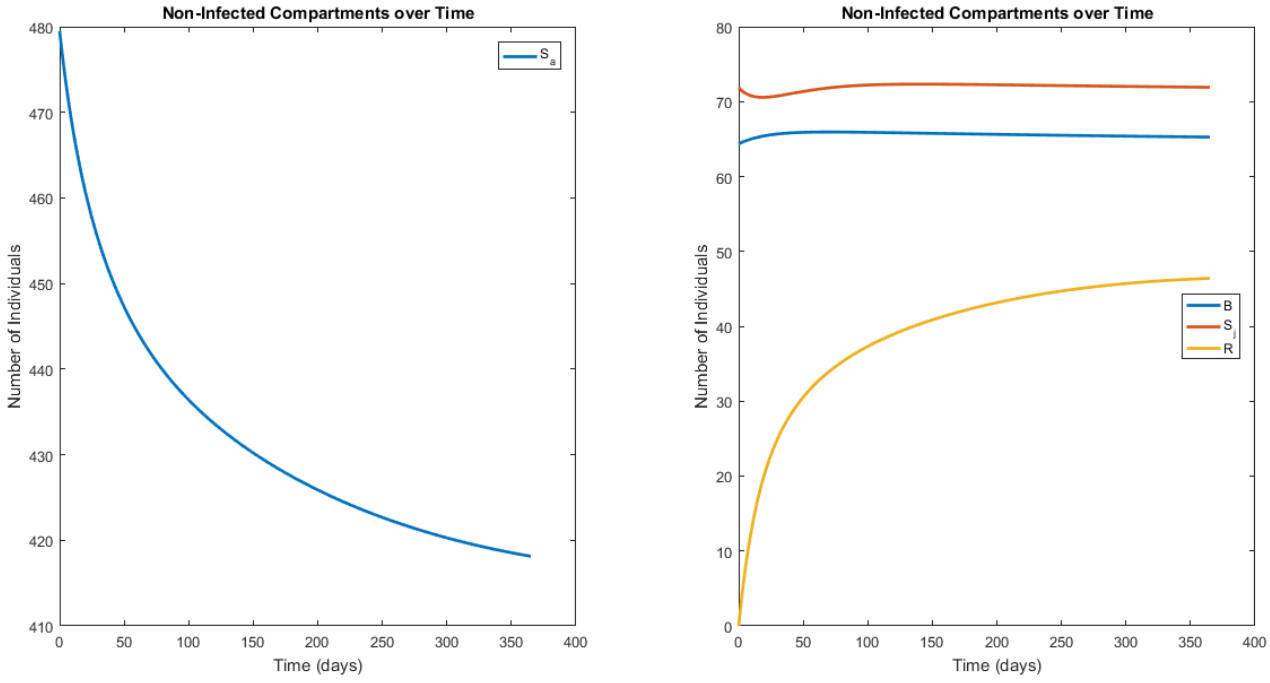

Figure 3: Plots showing the non-infected compartments with S_A on left and B, S_J, and R on right over a 365 day period.

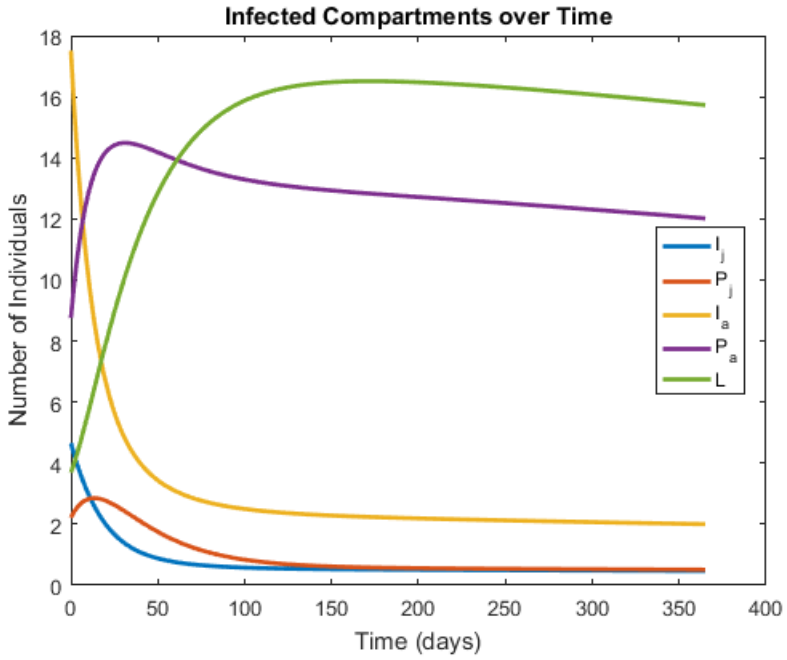

Figure 4: Plots showing the overall population in each infected compartment over a 365 day period.

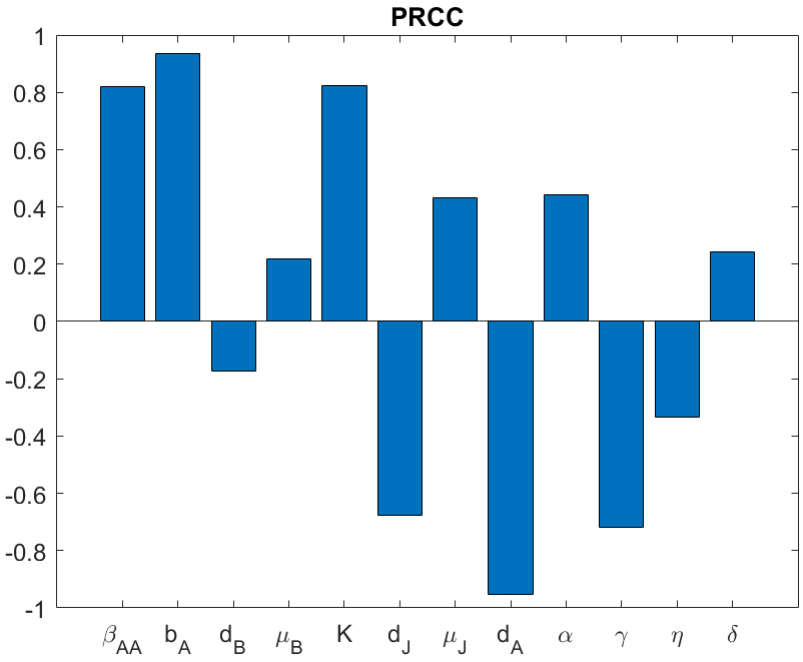

Figure 5: Chart showing the PRCC coefficients for model parameters determined using Latin Hypercube Sampling. All parameters had p-values less than 0.05 and were considered statistically significant.

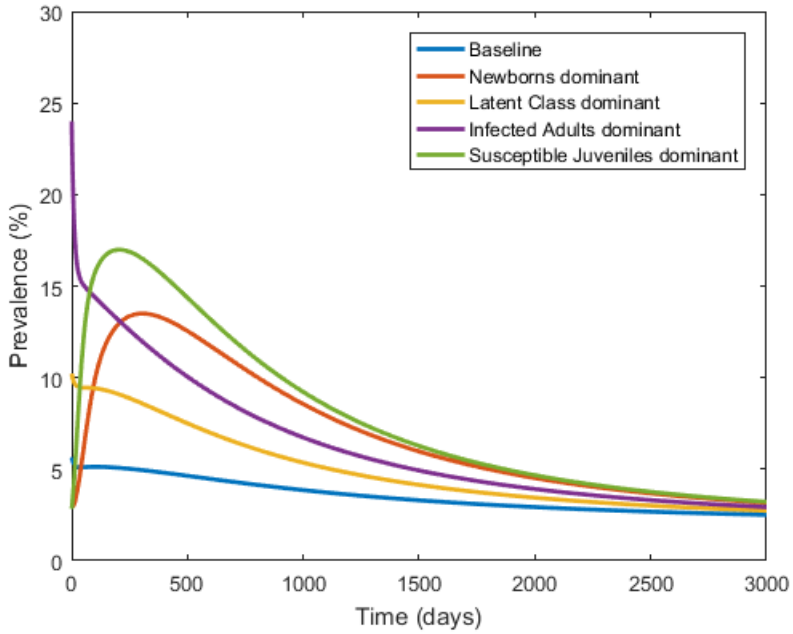

Figure 6: Graph showing the effect of different initial age structures on prevalence. The dominant initial class was the class that was set at 10 times its baseline value initially.

In order to compare the effect of the infected (I) and latent (L) classes on prevalence, the model was run at the disease free equilibrium to get a baseline for comparison. Then, one trial was run with the addition of 50 individuals in the I class and then with the addition of 50 individuals in the L class. Increases in the number of individuals in the latent class increased prevalence over the course of a year more than the acutely infected classes (Figure 7). This indicates that the latent class may be partially responsible for observed spikes in the number of infected individuals that have been observed in populations over time.

Next, we focus on transition rates in and out of our latent class. To study the effect of the transition rate δ from the latent class back to persistently infected class, simulations were run at different values of δ (Figure 8). Increases in δ caused significant increases in prevalence, as higher δ value results in a prevalence that is much higher than that corresponding to the baseline value $\delta = \frac{1}{60}$. This class has not been highly studied, however, our results demonstrate that it can have a large impact on the overall prevalence of hantavirus, which suggests it should be considered in future hantavirus models.

One can see the effect of the transition rate η from persistently infected class to the latent class in the results of simulations shown in Figure 9. As the rate η increases from $\eta = \frac{1}{56}$ to $\frac{1}{19}$, the prevalence doubles due to more individuals being able to transmit the virus.

In order to compare the effect of the recovered class, the recovery rate γ was altered 50% above and below the baseline conditions (Figure 10). The recovered class appears to have a large impact on the overall prevalence. When γ, the recovery rate, was varied by 50% above and below the baseline $\gamma = 1/10$ while keeping all other parameters constant, the overall prevalence ranged from 2% to 13%. When the rate of recovery was lowered to 1/15, the prevalence in the population was maintained at over twice the baseline value $\gamma = 1/10$. When it was increased to 1/5, the disease was eliminated from the population.

To understand the potential importance of the L latent compartment in this model, we ran a simulation without that class and compared the resulting prevalences. In Figure 11, the prevalence resulting from removing the L compartment is much higher than the prevalence found in our empirical data. Thus the L compartment may represent a reasonable mechanism in these dynamics.

4 Conclusions and Future Work

To understand the persistence of hantavirus in *A. montensis*, the rodent reservoir population represented by our data, we included a new non-infectious carrier class, L, into our model and investigated its effect on prevalence. In our model, individuals in this class (L) can transition back to the persistently infected, P_A, and begin to transmit the virus again. When the latent class is removed, the prevalence in the model is much higher (Figure 11) than that of our baseline model and the data set. The impact of the transition rates between latently infected and persistently infected adults is documented in Figures 8 and 9. Our simulation results indicate that this class may provide a potential explanation for the low prevalence endemicity observed in *A. montensis*

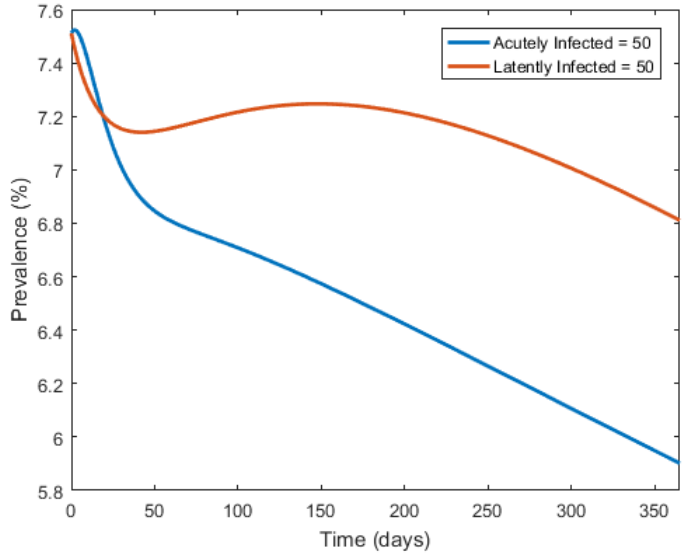

Figure 7: Graph comparing the effect of the latent and acutely infected classes on prevalence. These simulations were run at the disease free equilibrium, once with the addition of 50 individuals in the L class and once with the addition in the I class.

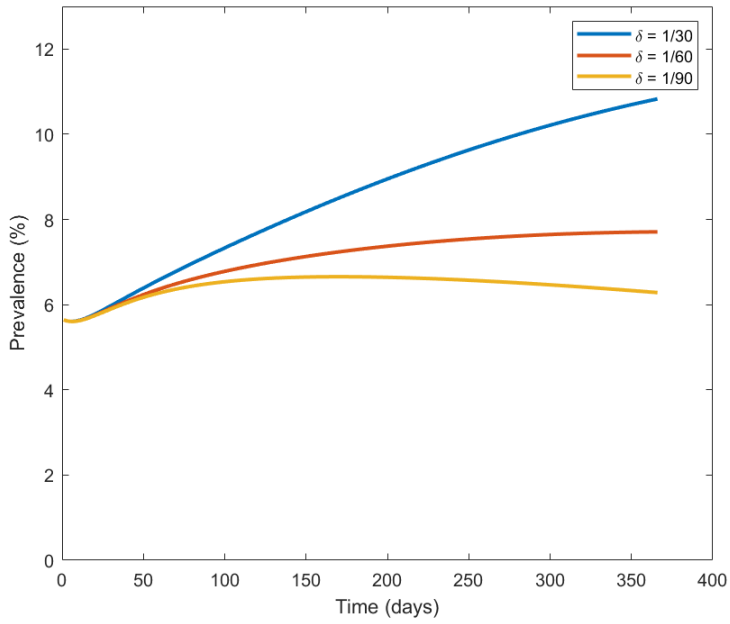

Figure 8: Graph showing the effect of the rate of transition δ on prevalence

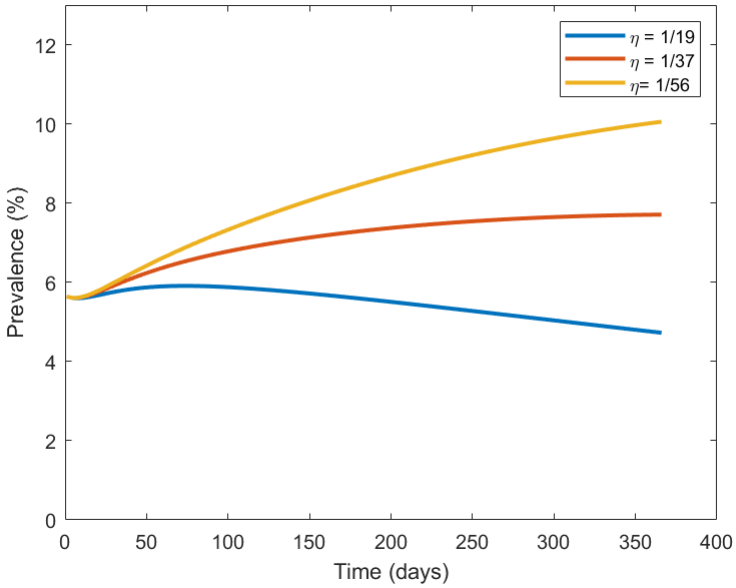

Figure 9: Graph showing the effect of the rate of transition η on prevalence

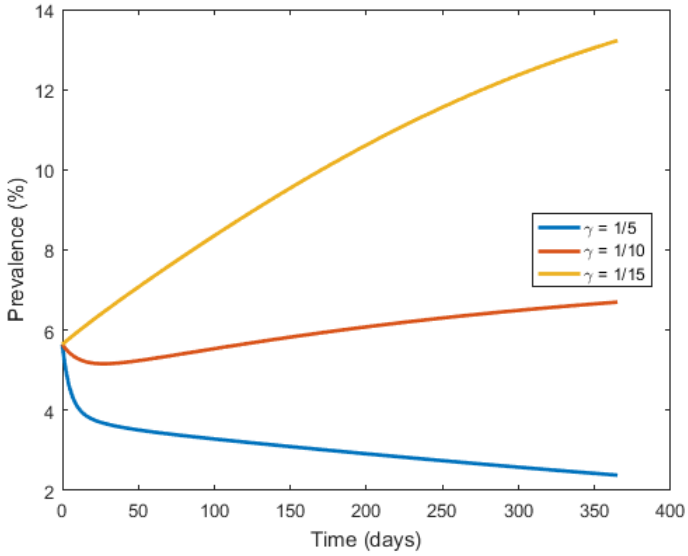

Figure 10: Graph showing the effect of varying the recovery rate γ on prevalence.

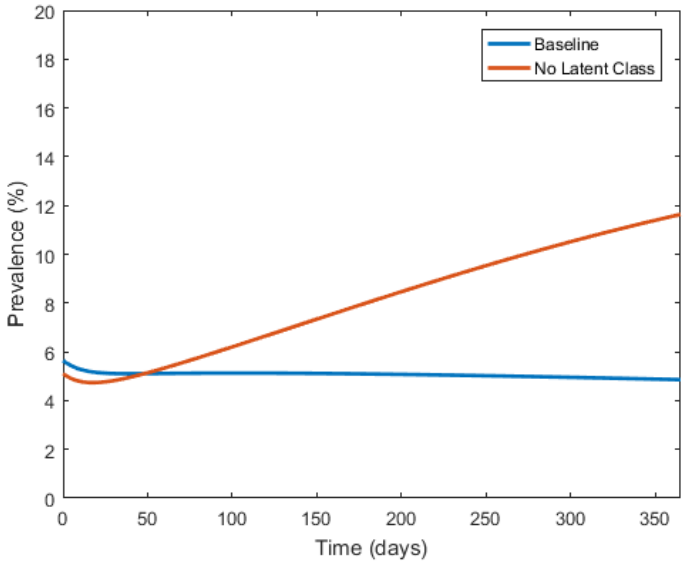

Figure 11: Graph comparing prevalence over a 365 day period for our model run at our baseline parameters 2 and with the latent class removed.

populations in the Mybaracyú Reserve, and other locations throughout Paraguay and South America.

The addition of a carrier class can lead to different endemic equilibrium scenarios, depending upon the force of infection, as seen in certain communicable diseases, such as HBV (Medley et al., 2001). When R_0 is high, infections are skewed to a younger age class, and in the opposing scenario with a lower R_0, infections are skewed to an older age class (Keeling and Rohani, 2008). Provided an age structured model, such as ours, and different initial conditions; a variety of endemic prevalence values are possible given different initial conditions. Although we only consider the parameters derived from our data set (and our model's robustness to those parameters (Figures 5, 7, 8, 9, 10), the literature documents a large range of observed prevalence values across various host species and environments (Childs et al., 1994; Teixeira et al., 2014). Motivated by low prevalence endemicity and modulations in prevalence, we created a model that incorporates both age structured population and carriers, which as previously noted, allows for endemicity with a wide array of parameter values. We also want to note that the transient dynamics observed when age structure is skewed suggest that factors affecting the age class distribution on a short-term timescale can heavily influence the prevalence. This result is very relevant to the observed endemicity at low percent prevalence (presumably when there is an adult age skew), and it also may explain the prevalence's correlation to seasonal, annual, or semi-annual outbreaks, as temporal modulations affect the resources that facilitate high fecundity and survival of young *A. montensis* (Sánchez Martínez, 2017). With an age structure that allows for sporadic outbreaks and a carrier class that serves as a long term reservoir, we were able to evaluate the prevalence of JABV over time within its rodent reservoir, *A. montensis*, and offer insight into various other hantavirus systems.

Our work with discrete models, though primarily focused upon the epidemiological status of individuals as well as the age structure of our sample population, could be built upon by other modeling techniques and additional heterogeneities. Environmental characteristics such as seasonality and landscape structure have been linked to increased prevalence, as have anthropogenic factors such as ecological disturbance and its corresponding impact on biodiversity (Langlois et al., 2001; Lehmer et al., 2008; Luis et al., 2010; Sánchez Martínez, 2017). Our model, which does not consider temporal variation, suggests that seasonal modulations are important for cyclical outbreaks (Figure 6), and it is well known that spatial arrangement of populations affects the endemicity and equilibrium prevalence of diseased populations (Gurarie and Seto, 2008; Hess, 1996; Wang and Mulone, 2003). Therefore, future work that considers spatial and temporal heterogeneity will complement our research, as well as past hantavirus modeling studies (Allen, McCormack, and Jonsson, 2006; Allen et al., 2009; Wesley et al., 2009, 2010). Additional research that considers anthropogenic and climate change, as well as optimal control strategies to limit zoonotic transfer during outbreaks will also contribute to the understanding and management of one of the deadliest viruses in the world.

5 Data Access

Note that no new data was used in this paper, and the data used here were from Eastwood et al. (2018).

Acknowledgments

This work was conducted during the 2016 Summer Research Experience (SRE) for undergraduates program at the National Institute for Mathematical and Biological Synthesis, an Institute sponsored by the National Science Foundation through NSF Award #DBI-1300426, with additional support from The University of Tennessee, Knoxville. Robert Owen was partially supported by the Programa Nacional de Incentivo a los Investigadores (CONACYT, Paraguay). Robert Owen and Colleen Jonsson were supported by NIH grant R01 AI103053. M. Igoe was supported by NIH/NIGMS-IMSD grant R25GM086761 and M. A. Rúa was supported by start-up funds from Wright State University. We would also like to thank Dr. Linda Allen, Dr. Jason Bintz, and Eric Carr for their assistance on our project.

References

Allen, L. J. S., E. J. Allen, and C. B. Jonsson (2006). The Impact of Environmental Variation on Hantavirus Infection in Rodents. In C. Castillo-Chavez and D. P. Clemence, and A. B. Gumel (Ed.), *Mathematical Studies on Human Disease Dynamics: Emerging Paradigms and Challenges*, Number 410 in AMS Contemporary Mathematics (CONM), pp. 1–15. Providence, RI: AMS. 128

Allen, L. J. S., R. K. McCormack, and C. B. Jonsson (2006). Mathematical models for hantavirus infection in rodents. *Bulletin of Mathematical Biology 68*(3), 511–524. 128, 139

Allen, L. J. S. and P. van den Driessche (2008). The basic reproduction number in some discrete-time epidemic models. *Journal of Difference Equations and Applications 14*(10–11), 1127–1147. 133

Allen, L. J. S., C. L. Wesley, R. D. Owen, D. G. Goodin, D. Koch, C. B. Jonsson, Y. K. Chu, J. M. S. Hutchinson, and R. L. Paige (2009). A habitat-based model for the spread of hantavirus between reservoir and spillover species. *Journal of Theoretical Biology 260*, 510–522. 128, 139

Bernshtein, A. D., N. S. Apekina, T. V. Mikhailova, Y. A. Myasnikov, L. A. Khlyap, Y. S. Korotkov, and I. N. Gavrilovskaya (1999). Dynamics of Puumala hantavirus infection in naturally infected bank voles (*Clethrinomys glareolus*). *Archives of Virology 144*(12), 2415–2428. 129

Borucki, M. K., J. D. Boone, J. E. Rowe, M. C. Bohlman, E. A. Kuhn, R. DeBaca, and S. C. S. Jeor (2000). Role of maternal antibody in natural infection of *Peromyscus maniculatus* with Sin Nombre virus. *Journal of Virology 74*(5), 2426–2429. 129

Botten, J. and E. A. Fix (2000). Experimental infection model for Sin Nombre hantavirus in the deer mouse (*Peromyscus maniculatus*). *Proceedings National Academy of Science USA 97*(19), 10578–10593. 127, 128

Calisher, C. H., K. D. Wagoner, B. R. Amman, J. J. Root, R. J. Douglass, A. J. Kuenzi, K. D. Abbott, C. Parmenter, T. L. Yates, T. G. Ksiazek, B. J. Beaty, and J. N. Mills (2007). Demographic factors associated with prevalence of antibody to Sin Nombre virus in deer mice in the western United States. *Journal of Wildlife Diseases 43*(1), 1– 11. 127

CDC (2016). Reported Cases of Hantavirus Disease. `http://www.cdc.gov/hantavirus/surveillance`. 128

Childs, J. E., T. G. Ksiazek, C. F. Spiropoulou, J. W. Krebs, S. Morzunov, G. O. Maupin, K. L. Gage, P. E. Rollin, J. Sarisky, R. E. Enscore, J. K. Frey, C. J. Peters, and S. T. Nichol (1994). Serologic and Genetic Identification of *Peromyscus maniculatus* as the Primary Rodent Reservoir for a New Hantavirus in the Southwestern United States. *Journal of Infectious Diseases 169*(6), 1271–1280. 128, 139

Dearing, M. D., M. A. Previtali, J. D. Jones, P. W. Ely, and B. A. Wood (2009). Seasonal variation in sin nombre virus infections in deer mice: preliminary results. *Journal of Wildlife Diseases 45*(2), 430–436. 129

Dohmae, K. and Y. Nishimune (1998). Maternal transfer of Hantavirus antibodies in rats. *Laboratory Animal Science 48*(4), 395–397. 129

Eastwood, G., J. V. Camp, Y. K. Chu, A. M. Sawyer, R. D. Owen, X. Cao, M. K. Taylor, L. Valdivieso-Torres, R. D. Sage, A. Yu, D. G. Goodin, V. J. Martinez-Bruyn, R. C. McAllister, L. Rodriguez, E. P. William, and C. B. Jonsson (2018). Habitat, species richness and hantaviruses of sigmodontine rodents within the Interior Atlantic Forest, Paraguay . *PLoS ONE 13*(8), e0201307. 127, 128, 129, 132, 139

Galiano, D., B. B. Kubiak, J. R. Marinho, and T. R. Ochotorena de Freitas (2011). Population dynamics of *Akodon montensis* and *Oligoryzomys nigripes* in an Araucaria forest of Southern Brazil . *Mammalia 77*(2), 173–179. 132

Gentile, R., P. S. D'Andrea, R. Cerqueira, and L. S. Maroja (2000). Population dynamics and reproduction of marsupials and rodents in a Brazilian rural area: a five-year study. *Studies on Neotropical Fauna and Environment 35*(1), 1–9. 132

Georges, C. G., F. Artunc, P. Weyrich, B. Friedrich, and S. C. Wolf (2008). Nephropathia epidemica as the result of a Puumala virus infection in a pregnant patient. *Deutsche Medizinische Wochenschrift 133*(37), 1830–1832. 129

Glass, G. E., J. E. Childs, G. W. Korch, and J. W. LeDuc (1988). Association of Intraspecific Wounding with Hantaviral Infection in Wild Rats (*Rattus norvegicus*). *Epidemiology and Infection 101*, 459–472. 127

Green, W. and E. Fix (1998). Tissue distribution of hantavirus antigen in naturally infected humans and deer mice. *Journal of Infectious Disease 177*(6), 1696–1700. 128

Gurarie, D. and E. Y. W. Seto (2008). Connectivity sustains disease transmission in environments with low potential for endemicity: modelling schistosomiasis with hydrologic and social connectivities . *Journal of the Royal Society Interface 6*, 495–508. 139

Hess, G. (1996). Disease in Metapopulation Models: Implications for Conservation . *Ecology 77*, 1617–1632. 139

Hutchinson, K. L. and E. A. Fix (1998). Pathogenesis of a North American hantavirus, Black Creek Canal virus, in experimentally infected *Sigmodon hispidus*. *American Journal of Tropical Medicine and Hygiene 59*(1), 58–65. 127

Hutchinson, K. L., P. E. Rollin, and C. J. Peters (2000). Transmission of Black Creek Canal virus between cotton rats. *Journal of Medical Virology 60*(1), 70–76. 127, 129

Jonsson, C. B., L. T. Figueiredo, and O. Vapalahti (2010). A global perspective on hantavirus ecology, epidemiology, and disease. *Clinical Microbiology Review 23*(2), 412–421. 127

Jordão, J. C., F. N. Ramos, and V. X. da Silva (2010). Demographic parameters of *Akodon montensis* (Mammalia: Rodentia) in an Atlantic Forest remnant of Southeastern Brazil. *Mammalia 74*, 395–400. 128

Kallio, E. R., M. Begon, H. Henttonen, E. Koskela, T. Mappes, A. Vaheri, and O. Vapalahti (2010). Hantavirus infections in fluctuating host populations: the role of maternal antibodies. *Proceedings of the Royal Society B: Biological Sciences 277*(1701), 3783–3791. 129

Kallio, E. R., H. Henttonen, E. Koskela, A. Lundkvist, T. Mappes, and O. Vapalahti (2013). Maternal antibodies contribute to sex-based difference in hantavirus transmission dynamics. *Biology Letters 9*(6), 20130887. 129

Kallio, E. R., A. Poikonen, A. Vaheri, O. Vapalahti, H. Henttonen, E. Koskela, and T. Mappes (2006). Maternal antibodies postpone hantavirus infection and enhance individual breeding success. *Proceedings of the Royal Society B: Biological Sciences 273*(1602), 2771–2776. 129

Keeling, M. J. and P. Rohani (2008). *Modeling Infectious Disease in Humans and Animals* . Princeton University Press. 139

Langlois, J. P., L. Fahrig, G. Merriam, and H. Artsob (2001). Landscape structure influences continental distribution of hantavirus in deer mice. *Landscape Ecology 16*(2), 255–266. 128, 139

LeDuc, J. W., J. E. Childs, and G. E. Glass (2002). The Hantaviruses, etiologic agents of hemorrhagic fever with renal syndrome: a possible cause of hypertension and chronic renal disease in the United States. *Annual Review of Public Health 13*, 79–98. 128

Lee, H. W., L. J. Baek, and K. M. Johnson (1982). Isolation of Hantaan virus, the etiologic agent of Korean hemorrhagic fever, from wild urban rats . *The Journal of Infectious Diseases 146*(5), 638–644. 132

Lehmer, E. M., C. A. Clay, J. Pearce-Duvet, S. St.Jeor, and M. D. Dearing (2008). Differential regulation of pathogens: the role of habitat disturbance in predicting prevalence of Sin Nombre virus. *Oecologia 155*, 429–439. 128, 139

Luis, A. D., R. J. Douglas, P. J. Hudson, J. N. Mills, and O. N. Bjornstad (2012). Sin Nombre hantavirus decreases survival of male deer mice. *Oceolgia 169*(1), 431–439. 127

Luis, A. D., R. J. Douglass, J. N. Mills, and O. N. Bjornstad (2010). The effects of seasonality, density and climate on the population dynamics of the Montana deer mice, important reservoir hosts for the Sin Nombre hantavirus. *Journal of Animal Ecology 79*, 462–470. 127, 128, 139

Marino, S., I. B. Hogue, C. J. Ray, and D. E. Kirschner (2009). A Methodology For Performing Global Uncertainty And Sensitivity Analysis In Systems Biology. *Journal of Theoretical Biology 254*(1), 178–196. 133

McAllister, R. C. and C. B. Jonsson (2014). Hantaviruses: past, present and future. *Future Virology 9*(1), 87 – 99. 128

Medley, G. F., N. A. Lindop, W. J. Edmunds, and D. J. Nokes (2001). Hepatitis-B virus endemicity: heterogeneity, catastrophic dynamics and control . *Nature Medicine 7*(5), 619–624. 139

Muylaert, R. L., R. S. Bovendorp, G. Sabino-Santos, Jr., P. R. Prist, G. L. Melo, C. d. F. Priante, D. A. Wilkinson, M. C. Ribeiro, and D. T. S. Hayman (2019). Hantavirus host assemblages and human disease in the Atlantic Forest . *PLOS Neglected Tropical Diseases 13*(8). 129

Owen, R. D., D. G. Goodin, D. E. Koch, Y. K. Chu, and C. B. Jonsson (2010). Spatiotemporal variation in *Akodon montensis* (*Cricetidae: Sigmodontinae*) and hantaviral seroprevalence in a subtropical forest ecosystem. *Journal of Mammology 91*(2), 467–481. 127, 128, 129, 132

Padula, P., R. Figueroa, M. Navarrete, E. Pizarro, R. Cadiz, C. Bellomo, C. Jofre, L. Zaror, E. Rodriguez, and R. Murúa (2004). Transmission Study of Andes Hantavirus Infection in Wild *Sigmodontine* Rodents. *Journal of Virology 78*(21), 11972–11979. 127, 128

Sánchez Martínez, J. P. (2017). Relación entre disturbios humanos ocasionados en el paisaje y la abundancia y otras medidas poblacionales de *Akodon montensis*, un hospedero de *Hantavirus* en Paraguay. Master's thesis, Universidad Nacional de Asunción, San Lorenzo, Paraguay. 139

Schountz, T., M. Acuña-Retamar, S. Feinstein, J. Prescott, F. Torres-Perez, B. Podell, S. Peters, C. Ye, W. C. Black IV, and B. Hjelle (2012). Kinetics of immune responses in deer mice experimentally infected with Sin Nombre virus. *Journal of Virology 86*(18), 10015–10027. 129

Schountz, T., S. Quackenbush, J. Rovnak, E. Haddock, W. C. Black IV, H. Feldmann, and J. Prescott (2014). Differential lymphocyte and antibody responses in deer mice infected with Sin Nombre hantavirus or Andes hantavirus. *Journal of Virology 88*(15), 8319–8331. 129

Teixeira, B. R., N. Loureiro, L. Strecht, R. Gentile, R. C. Oliveira, A. Guterres, J. Fernandes, L. H. B. V. Mattos, S. M. Raboni, G. Rubio, C. R. Bonvicino, C. N. Duarte dos Santos, E. R. S. Lemos, and P. S. D'Andrea (2014). Population Ecology of Hantavirus Rodent Hosts in Southern Brazil. *The American Journal of Tropical Medicine and Hygiene 91*(2), 249–257. 128, 132, 139

Voutilainen, L., E. R. Kallio, J. Niemimaa, O. Vapalahti, and H. Henttonen (2016). Temporal dynamics of Puumala hantavirus infection in cyclic populations of bank voles. *Scientific Reports 6*, 21323. 129

Wang, W. and G. Mulone (2003). Threshold of disease transmission in a patch environment . *Journal of Mathematical Analysis and Applications 285*, 321–335. 139

Wesley, C. L., L. J. S. Allen, C. B. Jonsson, Y. K. Chu, and R. D. Owen (2009). A discrete-time rodent-hantavirus model structured by infection and developmental stages. *Advanced Studies in Pure Mathematics 53*, 1–12. 128, 139

Wesley, C. L., L. J. S. Allen, and M. Langlais (2010). Models for the Spread and Persistence of Hantavirus Infection in Rodents with Direct and Indirect Transmission. *Mathematical Biosciences and Engineering 7*(1), 195–211. 128, 139

Yanagihara, R., H. L. Amyx, and D. Gajdusek (1985). Experimental infection with Puumala virus, the etiologic agent of *nephropathia epidemica*, in bank voles (*Clethrionomys glareolus*). *Journal of Virology 55*(1), 34–38. 127

Yates, T. L., J. N. Mills, C. A. Parmenter, T. G. Ksiazek, R. R. Parmenter, J. R. Vande-Castle, C. H. Calisher, S. T. Nichol, K. D. Abbott, J. C. Young, M. L. Morrison, B. J. Beaty, J. L. Dunnum, R. J. Baker, J. Salazar-Bravo, and C. J. Peters (2002). The Ecology and Evolutionary History of an Emergent Disease: Hantavirus Pulmonary Syndrome. *BioScience 52*(11), 989–998. 127